PHYSICAL REVIEW E **88**, 040701(R) (2013)

Hydrodynamic and subdiffusive motion of tracers in a viscoelastic medium

Denis S. Grebenkov,[1,*] Mahsa Vahabi,[1] Elena Bertseva,[2] László Forró,[2] and Sylvia Jeney[2]

[1]*Laboratoire de Physique de la Matière Condensée (UMR 7643), CNRS – Ecole Polytechnique, 91128 Palaiseau, France*

[2]*Laboratory of Physics of Complex Matter, Ecole Polytechnique Fédérale de Lausanne (EPFL), Station 3, CH-1015 Lausanne VD, Switzerland*

(Received 15 May 2013; revised manuscript received 25 July 2013; published 21 October 2013)

We investigate the diffusive motion of micron-sized spherical tracers in a viscoelastic actin filament network over the time span of 8 orders of magnitude using optical-tweezers single-particle tracking. The hydrodynamic interactions of a tracer with the surrounding fluid are shown to dominate at microsecond time scales, while subdiffusive scaling due to viscoelastic properties of the medium emerges at millisecond time scales. The transition between these two regimes is analyzed in the frame of a minimal phenomenological model which combines the Basset force and the generalized Stokes force. The resulting Langevin equation accounts for various dynamical features of the thermal motion of endogenous or exogenous tracers in viscoelastic media such as inertial and hydrodynamic effects at short times, subdiffusive scaling at intermediate times, and eventual optical trapping at long times. Simple analytical formulas for the mean-square displacement and velocity autocorrelation function are derived.

DOI: 10.1103/PhysRevE.88.040701 PACS number(s): 87.16.Ka, 05.40.−a, 02.50.Ey, 05.10.Gg

Single-particle tracking (SPT) techniques allow us to survey individual trajectories of organelles, vesicles, macromolecules, or artificial tracers for inferring the most detailed information about their dynamics in complex or viscoelastic media, notably in living cells [1–8]. The statistical analysis of these random trajectories gives access not only to local dynamical quantities [e.g., mean-square displacement (MSD) or velocity autocorrelation function (VACF)] and microrheological quantities (e.g., shear moduli or stiffness), but also to their fluctuations and heterogeneities within a sample. In particular, the microrheological properties of semiflexible polymers have been intensively studied at acquisition rates up to hundreds of Hz by video tracking and up to tens of kHz by optical tweezers [9,10]. However, to get the full picture of the viscoelastic response of a complex medium, it is of primary importance to perform measurements in a broad time domain. In this Rapid Communication, we report the acquisition of SPT over eight orders of magnitude, from 1 μs to 50 s. The high temporal resolution allows us to reveal the importance of hydrodynamic interactions of a tracer with the surrounding fluid that dominate at microsecond time scales. In turn, the viscoelastic properties of actin filaments lead to subdiffusive scaling at longer, millisecond time scales.

The experimental setup has been described in [11,12]. The actin filaments were reconstituted from the preformed actin filaments (Cytoskeleton, Inc. AKF99-A) by dissolving in 2 ml of Milli-Q water. This gave the concentration of 0.5 mg/ml in the following buffer: 6 mM Tris-HCl pH 8.0, 0.24 mM $CaCl_2$, 0.24 mM ATP, 2.4 mM $MgCl_2$, and 6% (wt/vol) sucrose. The 3 μm diameter melamine resin beads (Microparticles GmbH, S1712) were added to water beforehand. The actin filaments with beads were placed between a microscope slide and a coverslip separated by 200 μm spacers. The obtained sample chamber was divided into two parts: one for actin, and the other for pure water. Both solutions contained the same kind of tracers.

The time-averaged (TA) MSD and TA VACF were calculated separately for each bead as

$$\mathcal{M}(n\delta) \equiv \frac{1}{N-n}\sum_{k=1}^{N-n}[X((k+n)\delta) - X(k\delta)]^2, \tag{1}$$

$$\mathcal{V}(n\delta) \equiv \frac{\delta^{-2}}{N-n-1}\sum_{k=1}^{N-n-1}[X((k+1)\delta) - X(k\delta)] \times [X((k+n+1)\delta) - X((k+n)\delta)], \tag{2}$$

where $X(t)$ is the coordinate of the bead at time t, N is the number of points of the acquired trajectory, $n\delta$ is the lag time, and δ is the time step of data acquisition. In the setup, $\delta = 1$ μs and $N = 5 \times 10^7$ (50-s-long trajectories). In the linearity range of the position detecting system, $X(t)$ is proportional to the position fluctuation signal $S(t)$ recorded in volts: $X(t) = \beta S(t)$, where β is the volt-to-meter conversion factor.

The measurements in water served as a reference for calibration of the trap. For this purpose, the TA MSD was fitted by the function $2k_BT\beta^2 G^{(1)}(t)$, where k_B is the Boltzmann constant, T the absolute temperature, and $G^{(1)}(t)$ the normalized ensemble-averaged MSD for a tracer in water [25] [see also Eq. (11) with $p = q = 2$ below]. The other parameters were $\rho_f = 1000$ kg/m^3 (water density), $\rho = 1510$ kg/m^3 (melamine resin density), $\eta = 0.959 \times 10^{-3}$ kg/m s (dynamic viscosity of water at $T = 295$ K), and $a = 1.5$ μm (bead radius). The only fitting parameters were the spring constant k of the laser optical trap and the factor β. For two laser powers used, we obtained $k_1 = 3.77 \times 10^{-6}$ N/m (weak trap) and $k_2 = 1.28 \times 10^{-5}$ N/m (strong trap). Once the spring constant k was determined in water, the conversion factors β for beads in the actin filament solution were fixed by setting the long-time plateau value of the TA MSDs to $2k_BT/k$, according to the principle of equipartition of energy.

Figure 1 shows the TA MSD and TA VACF of a spherical tracer in an actin filament solution. The first group of blue

*denis.grebenkov@polytechnique.edu

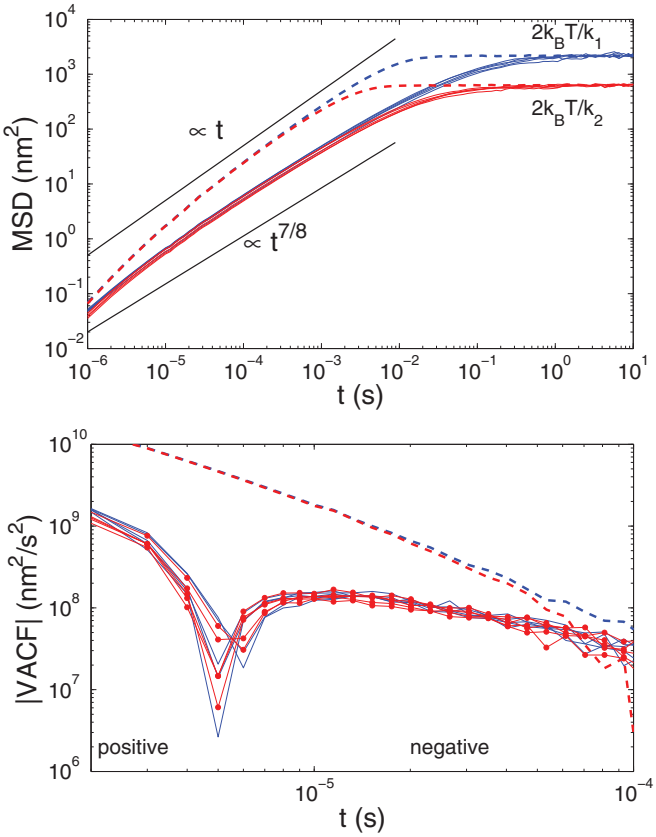

FIG. 1. (Color online) Experimental TA MSD and TA VACF of a spherical tracer in water (dashed curves) and in an actin filament solution for the weak (group of blue solid curves) and strong (group of red solid curves) optical traps, with trap constants $k_1 = 3.77 \times 10^{-6}$ N/m and $k_2 = 1.28 \times 10^{-5}$ N/m, respectively. Five curves in each group show the results for five trajectories. Red full circles are added for the VACF plot to better distinguish the two groups. Two black solid lines indicate the MSD slopes 1 and 7/8 for normal and anomalous diffusions. The actin concentration is 0.5 mg/ml, the temperature is $T = 295$ K.

solid curves corresponds to five trajectories in the weak optical trap, while the second group of red curves corresponds to five trajectories in the strong optical trap. The curves from each group are close to each other (small deviations between curves within one group can be attributed to heterogeneities in the actin filament solution). Note also that the curves from both groups are close to each other at small times at which the optical trap is negligible. For comparison, the TA MSD and TA VACF for the same bead in water are shown by dashed lines. At millisecond time scales, the diffusive motion in water (with a linear scaling of MSD versus lag time) can be distinguished from the subdiffusive dynamics of tracers in an actin filament solution (for which MSD scales as t^α, with $\alpha \approx 7/8$). At shorter, microsecond time scales, MSD curves for both diffusive and subdiffusive dynamics exhibit deviations that can be attributed to inertial effects and hydrodynamic interactions of a tracer with the surrounding fluid. The importance of these effects is particularly clear from the TA VACF curves which change the sign at $t_c \approx 5$ μs. For $t > t_c$, the viscoelastic properties of the medium dominate and lead to antipersistent dynamics (with negative correlations of displacements). The motion becomes persistent for $t < t_c$ due to inertial and hydrodynamic effects.

To investigate the transition between these two regimes, we propose a phenomenological model which combines the generalized Stokes force and the Basset force. The generalized Stokes force with a friction memory kernel $\gamma_\alpha(t)$,

$$F_S(t) = -\int_{-\infty}^{t} dt' \gamma_\alpha(t-t')\dot{X}(t'), \tag{3}$$

was suggested for describing general open systems [13,14]. Lately, this description has also become common for incorporating viscoelastic properties of a medium [8,15–21]. In particular, a slowly decaying kernel $\gamma_\alpha(t) = \frac{\gamma_\alpha}{\Gamma(1-\alpha)} t^{-\alpha}$ with an exponent $0 < \alpha < 1$ leads to subdiffusive scaling of the MSD with the same exponent α.

In turn, the Basset force describes hydrodynamic interactions of a spherical tracer of radius a with the surrounding fluid [22]

$$F_B(t) = -\frac{2}{3}\pi a^3 \rho_f \ddot{X} - 6a^2\sqrt{\pi\rho_f\eta}\int_{-\infty}^{t} dt' \frac{\ddot{X}(t')}{\sqrt{t-t'}}, \tag{4}$$

where ρ_f and η are the fluid density and viscosity. The hydrodynamic interactions which appear at short time scales have been thoroughly investigated in viscous media, theoretically [23–27] and experimentally [28–30].

Combining these two parts, the resulting generalized Langevin equation (GLE) for the random trajectory $X(t)$ of a tracer of mass m diffusing in a harmonic potential of the laser trap is

$$m\ddot{X}(t) = F(t) + F_S(t) + F_B(t) - kX(t), \tag{5}$$

where $F(t)$ is the thermal force. Since experimental data are available from a starting time (which we set to 0), one employs the causality principle to cut the integrals in Eqs. (4) and (3) below 0. Applying the standard technique of forward and inverse Laplace transforms to this linear GLE, one gets a formal solution as [20,21]

$$X(t) = X_0(t) + \int_0^t dt' G(t-t')F(t'), \tag{6}$$

in which the deterministic term $X_0(t)$ (depending on the initial conditions) and the stochastic term are both determined by the linear response function $G(t)$ which is defined through its inverse Laplace transform

$$\tilde{G}(s) = [ms^2 + \tilde{\gamma}(s)s + k]^{-1}, \tag{7}$$

where the effective friction kernel $\tilde{\gamma}(s)$ includes both the hydrodynamic interactions and subdiffusive scaling: $\tilde{\gamma}(s) = \frac{1}{2}m_f s + \gamma_h s^{1/2} + \gamma_\alpha s^{\alpha-1}$, with $\gamma_h = 6\pi a^2\sqrt{\rho_f\eta}$ for a purely viscous medium, and $m_f = 4\pi a^3\rho_f/3$ being the mass of the fluid displaced by the tracer. Both coefficients γ_α and γ_h are related to the viscosity of the medium. However, finding this relation for viscoelastic media would require a microscopic model for hydrodynamic interactions that is beyond the scope of the Rapid Communication.

When the thermal force $F(t)$ is Gaussian, its distribution is fully characterized by its mean, $\langle F(t)\rangle = 0$, and the covariance which is related to the frictional part through the fluctuation-dissipation theorem: $\langle F(t)F(t')\rangle = k_B T\gamma(|t-t'|)$ [31]. In

that case, all the dynamical properties are fully determined by the effective kernel $\gamma(t)$ or, equivalently, by $G(t)$. In particular, the exact formulas for the MSD and VACF from [20,21] can be approximated as

$$\langle [X(t_1) - X(t_2)]^2 \rangle \simeq 2k_B T G^{(1)}(|t_1 - t_2|), \quad (8)$$

$$\langle \dot{X}(t_1)\dot{X}(t_2) \rangle \simeq k_B T g(|t_1 - t_2|), \quad (9)$$

where $g(t)$ and $G^{(1)}(t)$ are the derivative and the primitive of $G(t)$, respectively (the influence of correction terms was studied in [21]). For long trajectories, these ensemble-averaged MSD and VACF can be used for fitting $\mathcal{M}(t)$ and $\mathcal{V}(t)$.

The practical use of the explicit relations (8) and (9) requires computing the inverse Laplace transform of $\tilde{G}(s)$. Except for a few particular or limiting cases, no analytical representation of $G(t)$ is suitable for fitting experimental curves in the presence of the long memory friction kernel (i.e., with $0 < \alpha < 1$). To overcome this problem, several shortcuts have been proposed such as using the Laplace transform of the experimental MSD [32] or "bypassing the foray into Laplace space" through the Fourier transform [33].

In this Rapid Communication, we derive an accurate explicit representation of the linear response function $G(t)$ and, consequently, of the related quantities such as the MSD and VACF. The following approach resolves a long-standing problem of finding explicit solutions of the GLE in the presence of subdiffusive scaling. For this purpose, we approximate the scaling exponent α by a rational number p/q, with integer p and q. Changing s to a new variable $z = (s\tau)^{1/q}$ (with τ being an appropriate time scale) allows one to represent the nonanalytic function $1/\tilde{G}(s)$ of s as a polynomial $P(z)$ of degree $2q$

$$\frac{\tau^2}{M\tilde{G}(s)} \equiv P(z) = z^{2q} + \frac{\gamma_h\sqrt{\tau}}{M} z^{3q/2} + \frac{\gamma_\alpha \tau^{2-\alpha}}{M} z^p + \frac{k\tau^2}{M},$$

where $M = m + m_f/2$ is the effective mass (note that $3q/2$ is an integer by setting q to be even). For convenience, we choose the time scale τ by setting the coefficient in front of z^p to 1: $\tau = (M/\gamma_\alpha)^{1/(2-\alpha)}$. The above polynomial has $2q$ (complex-valued) roots z_j. In a general situation, all the roots are distinct (i.e., $z_j \neq z_k$ for $j \neq k$) so that one gets $\frac{M}{\tau^2}\tilde{G}(s) = \sum_{j=1}^{2q} \frac{A_j}{z - z_j}$, with the coefficients $A_j = \prod_{k\neq j}^{2q} (z_j - z_k)^{-1}$, from which the inverse Laplace transform yields

$$G(t) = \frac{\tau}{M} \sum_{j=1}^{2q} A_j (t/\tau)^{\frac{1}{q}-1} E_{\frac{1}{q},\frac{1}{q}}(z_j (t/\tau)^{\frac{1}{q}}), \quad (10)$$

where $E_{\alpha,\beta}(z)$ is the Mittag-Leffler function [34,35]. From this expression, one deduces the analytical formulas for $G^{(1)}(t)$ and $g(t)$ which are related to the MSD and VACF through Eqs. (8) and (9):

$$G^{(1)}(t) = \frac{\tau^2}{M} \sum_{j=1}^{2q} A_j (t/\tau)^{\frac{1}{q}} E_{\frac{1}{q},\frac{1}{q}+1}(z_j (t/\tau)^{\frac{1}{q}}), \quad (11)$$

$$g(t) = \frac{1}{M} \sum_{j=1}^{2q} A_j (t/\tau)^{\frac{1}{q}-2} E_{\frac{1}{q},\frac{1}{q}-1}(z_j (t/\tau)^{\frac{1}{q}}). \quad (12)$$

The integral representation of Mittag-Leffler functions [34] can be used for a rapid and accurate numerical computation of $G^{(1)}(t)$ and $g(t)$.

The above model includes the known explicit solutions:

(i) Normal diffusion of a massive tracer ($\alpha = 1$ and $\gamma_h = 0$) corresponds to $p = q = 1$ for which $E_{1,1}(z) = e^z$ and thus $G(t) = (A_1 e^{z_1\gamma_1 t/M} + A_2 e^{z_2\gamma_1 t/M})/\gamma_1$, with $z_{1,2} = -\frac{1}{2}(1 \pm \sqrt{1 - 4kM/\gamma_1^2})$. When $M \to 0$, the linear response function reduces to $G(t) = e^{-kt/\gamma_1}/\gamma_1$.

(ii) Normal diffusion of a massive tracer with hydrodynamic interactions ($\alpha = 1$ and $\gamma_h \neq 0$) is obtained for $p = q = 2$, for which functions $E_{\frac{1}{2},\frac{n}{2}}(z)$ can be expressed through $E_{\frac{1}{2},1}(z) = e^{z^2}\mathrm{erfc}(-z)$ which yields the classical formulas for the MSD and VACF [25,30] [here $\mathrm{erfc}(z)$ is the complementary error function].

(iii) When there is no optical trapping ($k = 0$), some roots z_j are zero so that one gets another representation $\frac{M}{\tau^2}\tilde{G}(s) = \frac{1}{z^p}\sum_j \frac{\bar{A}_j}{z - z_j}$, in which $\bar{A}_j = \prod_{k\neq j}(z_j - z_k)^{-1}$ and the sum and product are taken over all nonzero roots z_j of the polynomial $P(z)$. The Laplace inversion of this relation yields

$$G(t) = \frac{\tau}{M} \sum_j \bar{A}_j (t/\tau)^{\frac{1+p}{q}-1} E_{\frac{1}{q},\frac{1+p}{q}}(z_j (t/\tau)^{\frac{1}{q}}), \quad (13)$$

from which

$$G^{(1)}(t) = \frac{\tau^2}{M} \sum_j \bar{A}_j (t/\tau)^{\frac{1+p}{q}} E_{\frac{1}{q},\frac{1+p}{q}+1}(z_j (t/\tau)^{\frac{1}{q}}),$$

$$g(t) = \frac{1}{M} \sum_j \bar{A}_j (t/\tau)^{\frac{1+p}{q}-2} E_{\frac{1}{q},\frac{1+p}{q}-1}(z_j (t/\tau)^{\frac{1}{q}}). \quad (14)$$

The classical formulas for $\alpha = 1$ can be retrieved by setting again $p = q = 2$ [23,24]. In turn, for subdiffusion with $\gamma_h = 0$, the above formula reduces to $G(t) = \frac{t}{M} E_{2-\alpha,2}(-(t/\tau)^{2-\alpha})$ [20,21].

Using the properties of Mittag-Leffler functions and relations for the roots z_j of the polynomial $P(z)$, one can derive the asymptotic behavior of $G(t)$ (and thus the MSD and VACF) at different time scales (Fig. 2):

$$G(t) \simeq \frac{t}{M} - \frac{4\gamma_h t^{\frac{3}{2}}}{3\sqrt{\pi}M^2} + \frac{\gamma_h^2 t^2}{2M^3} - \frac{8\gamma_h^3 t^{\frac{5}{2}}}{15\sqrt{\pi}M^4} + \cdots \quad (t \ll \tau_h),$$

$$G(t) \simeq \frac{t^{\alpha-1}}{\gamma_\alpha \Gamma(\alpha)} - \frac{\gamma_h t^{2\alpha-\frac{5}{2}}}{\gamma_\alpha^2 \Gamma(2\alpha - \frac{3}{2})} + \cdots \quad (\tau \ll t \ll \tau_k),$$

$$G(t) \simeq \frac{\gamma_\alpha t^{-\alpha-1}}{|\Gamma(-\alpha)|k^2} + \frac{\gamma_\alpha^2 t^{-2\alpha-1}}{\Gamma(-2\alpha)k^3} - \frac{3\gamma_h t^{-\frac{5}{2}}}{4\sqrt{\pi}k^2} + \cdots \quad (t \gg \tau_k),$$

where $\tau_k = (\gamma_\alpha/k)^{1/\alpha}$ is the trapping time and $\tau_h = (M/\gamma_h)^2$ is the characteristic time for hydrodynamic interactions. For normal diffusion ($\alpha = 1$), one retrieves the classical behavior $g(t) \simeq \frac{\gamma_h}{2\sqrt{\pi}\gamma_1^2} t^{-3/2}$ [23] for $k = 0$ and $g(t) \simeq \frac{15\gamma_h}{8\sqrt{\pi}k^2} t^{-7/2}$ for $k > 0$ [25].

Searching for a minimal phenomenological model to describe the motion of spherical tracers in viscoelastic media, one may question whether the inclusion of the hydrodynamic interactions was relevant or not. For a massless tracer, the theoretical TA MSD and TA VACF are $\frac{2k_B T}{k}[1 - E_{\alpha,1}(-kt^\alpha/\gamma_\alpha)]$

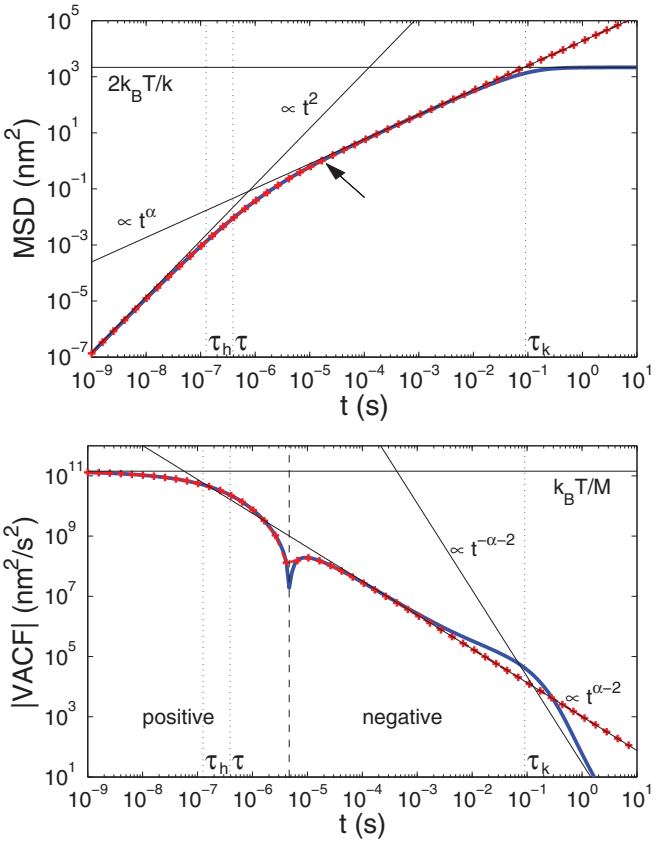

FIG. 2. (Color online) Theoretical TA MSD and TA VACF of a spherical tracer in a viscoelastic medium. Curves from Eqs. (11) and (12) are shown by a thick solid blue line ($\alpha = 7/8$, $k = 3.77 \times 10^{-6}$ N/m, $\gamma_\alpha = 4.6 \times 10^{-7}$ kg/s$^{9/8}$, $\gamma_h = 8.0 \times 10^{-11}$ kg/s$^{1/2}$, $M = 2.84 \times 10^{-14}$ kg); curves from Eqs. (14) without optical trapping ($k = 0$) are shown by red crosses, and the asymptotic behaviors at different time scales are shown by thin black lines. Vertical dotted lines locate three characteristic time scales: $\tau_h = (M/\gamma_h)^2$, $\tau = (M/\gamma_\alpha)^{1/(2-\alpha)}$, and $\tau_k = (\gamma_\alpha/k)^{1/\alpha}$, while the vertical dashed line separates the regions with positive and negative values of the TA VACF. The arrow indicates the region where the inertial and hydrodynamic effects lead to deviations from the subdiffusive scaling.

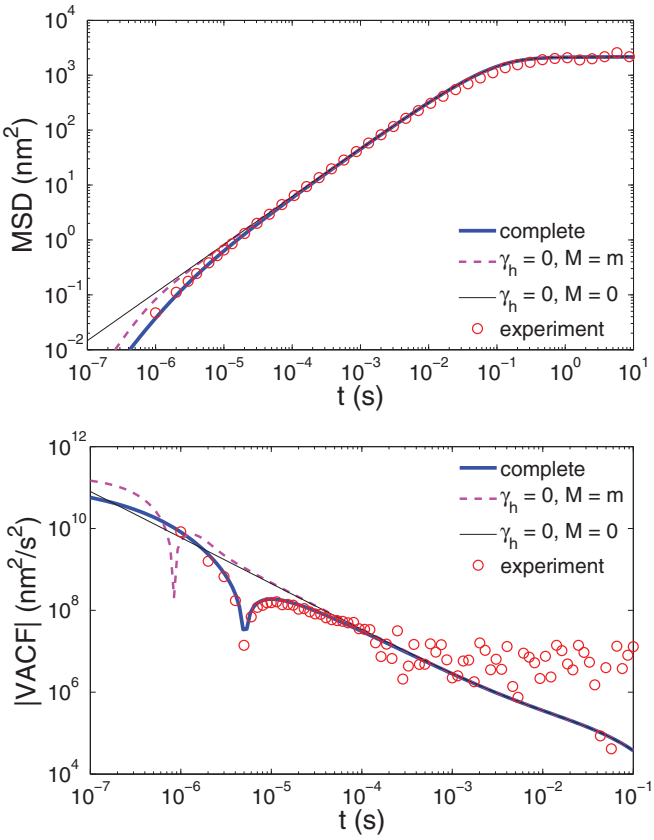

FIG. 3. (Color online) Experimental TA MSD and TA VACF of a spherical tracer in an actin filament solution (circles) compared with three theoretical models: the complete model (anomalous diffusion with hydrodynamic interactions; shown by solid blue curve), and its two simplified versions, in which the hydrodynamic interactions and then the inertial effects are neglected. The model parameters are $k = 3.77 \times 10^{-6}$ N/m, $\alpha = 7/8$, $\gamma_\alpha = 4.38 \times 10^{-7}$ kg/s$^{9/8}$, $\gamma_h = 8.0 \times 10^{-11}$ kg/s$^{1/2}$, $M = 2.84 \times 10^{-14}$ kg. The actin concentration is 0.5 mg/ml, the temperature is $T = 295$ K.

and $\frac{k_B T}{\gamma_\alpha} t^{\alpha-2} E_{\alpha,\alpha-1}(-kt^\alpha/\gamma_\alpha)$, which for short times behave as $\frac{2D_\alpha}{\Gamma(\alpha+1)} t^\alpha$ and $\frac{-D_\alpha}{|\Gamma(\alpha-1)|} t^{\alpha-2}$, where $D_\alpha = k_B T/\gamma_\alpha$ is the generalized diffusion coefficient [20,21]. In particular, the above TA VACF would be always negative showing antipersistence in random displacements of a massless tracer. On the contrary, the experimental TA VACF in Fig. 1 clearly exhibits the change of sign at $t_c \approx 5\ \mu$s that requires accounting for inertial and hydrodynamic effects. However, would it be sufficient to include only the inertial term ms^2 but neglect the hydrodynamic term $\gamma_h s^{3/2}$? Figure 3 illustrates the importance of the hydrodynamic interactions. We compare the experimental TA MSD and TA VACF (circles) for one trajectory with the theoretical curves obtained from the complete model (i.e., when both the inertial and hydrodynamic effects are included), and two simplified models, in which one first neglects the hydrodynamic interactions (setting $\gamma_h = 0$ and $M = m$) and then ignores inertial effects (setting $\gamma_h = 0$ and $M = 0$). One can see that the theoretical TA MSD and TA VACF from Eqs. (11) and (12) (referred to as complete model) correctly reproduce the experimental ones over seven orders of magnitude in time (the range being narrower for the TA VACF, for which the experimental values become hidden by intrinsic fluctuations at $t > 10^{-4}$ s). Deviations between complete and simplified models for the TA MSD are relatively small though visible for the lag time around 1 μs (the range accessible in our experiment). In turn, the deviations are much more explicit for the TA VACF. We conclude that the hydrodynamic interactions become significant for big tracers (of radius above 1 micron) and at time scales below tens of microseconds. The explicit formulas (11) and (12) allow one to reveal the respective roles of various forces and mechanisms and to choose the appropriate model for a reliable analysis of SPT trajectories of endogenous or artificial tracers in complex viscoelastic media such as polymer networks and living cells.

In conclusion, we presented an optical-tweezers experiment in which the hydrodynamic interactions and subdiffusive scaling in an actin filament solution manifest simultaneously. We proposed a minimal phenomenological model in which intricate interactions of a tracer with the fluid and actin

filaments are effectively characterized by the Basset force and the generalized Stokes force, respectively. From this model, we derived simple analytical formulas for the TA MSD and TA VACF that allowed us to accurately fit experimental data and characterize the underlying dynamics over the time span of eight orders of magnitude, from 1 μs to tens of seconds.

[1] I. M. Tolić-Nørrelykke, E.-L. Munteanu, G. Thon, L. Oddershede, and K. Berg-Sørensen, Phys. Rev. Lett. **93**, 078102 (2004).
[2] I. Golding and E. C. Cox, Phys. Rev. Lett. **96**, 098102 (2006).
[3] D. Arcizet, B. Meier, E. Sackmann, J. O. Rädler, and D. Heinrich, Phys. Rev. Lett. **101**, 248103 (2008).
[4] C. Wilhelm, Phys. Rev. Lett. **101**, 028101 (2008).
[5] D. Wirtz, Ann. Rev. Biophys. **38**, 301 (2009).
[6] J. Szymanski and M. Weiss, Phys. Rev. Lett. **103**, 038102 (2009).
[7] J.-H. Jeon, V. Tejedor, S. Burov, E. Barkai, C. Selhuber-Unkel, K. Berg-Sørensen, L. Oddershede, and R. Metzler, Phys. Rev. Lett. **106**, 048103 (2011).
[8] E. Bertseva, D. S. Grebenkov, P. Schmidhauser, S. Gribkova, S. Jeney, and L. Forró, Eur. Phys. J. E **35**, 63 (2012).
[9] F. Gittes, B. Schnurr, P. D. Olmsted, F. C. MacKintosh, and C. F. Schmidt, Phys. Rev. Lett. **79**, 3286 (1997).
[10] F. Gittes and F. C. MacKintosh, Phys. Rev. E **58**, R1241 (1998).
[11] E. Bertseva *et al*., Nanotechnology **20**, 285709 (2009).
[12] S. Jeney, F. Mor, R. Koszali, L. Forró, and V. T. Moy, Nanotechnology **21**, 255102 (2010).
[13] H. Mori, Prog. Theor. Phys. **33**, 423 (1965).
[14] M. H. Lee, Phys. Rev. E **62**, 1769 (2000).
[15] J. M. Porrà, K.-G. Wang, and J. Masoliver, Phys. Rev. E **53**, 5872 (1996).
[16] K. G. Wang and M. Tokuyama, Phys. A **265**, 341 (1999).
[17] E. Lutz, Phys. Rev. E **64**, 051106 (2001).
[18] N. Pottier, Physica A **317**, 371 (2003).
[19] A. D. Vinales and M. A. Desposito, Phys. Rev. E **73**, 016111 (2006).
[20] M. A. Desposito and A. D. Vinales, Phys. Rev. E **80**, 021111 (2009).
[21] D. S. Grebenkov, Phys. Rev. E **83**, 061117 (2011).
[22] A. B. Basset, *A Treatise on Hydrodynamics, With Numerous Examples* (Deighton, Bell and Co., Cambridge, England, 1888).
[23] A. Widom, Phys. Rev. A **3**, 1394 (1971).
[24] E. J. Hinch, J. Fluid Mech. **72**, 499 (1975).
[25] H. J. H. Clercx and P. P. J. M. Schram, Phys. Rev. A **46**, 1942 (1992).
[26] F. Mainardi and P. Pironi, Extr. Math. **11**, 140 (1996).
[27] T. Indei, J. D. Schieber, and A. Córdoba, Phys. Rev. E **85**, 041504 (2012).
[28] T. Franosch, M. Grimm, M. Belushkin, F. M. Mor, G. Foffi, L. Forró, and S. Jeney, Nature **478**, 85 (2011).
[29] R. Huang, I. Chavez, K. M. Taute, B. Lukić, S. Jeney, M. G. Raizen, and E.-L. Florin, Nat. Phys. **7**, 576 (2011).
[30] M. Grimm, T. Franosch, and S. Jeney, Phys. Rev. E **86**, 021912 (2012).
[31] R. Kubo, M. Toda, and N. Hashitsume, *Statistical Physics II. Nonequilibrium Statistical Mechanics* (Springer, New York, 1985).
[32] T. G. Mason and D. A. Weitz, Phys. Rev. Lett. **74**, 1250 (1995).
[33] R. M. L. Evans, M. Tassieri, D. Auhl, and T. A. Waigh, Phys. Rev. E **80**, 012501 (2009).
[34] R. Gorenflo, J. Loutchko, and Y. Luchko, Fract. Calc. Appl. Anal. **5**, 491 (2002).
[35] H. J. Haubold, A. M. Mathai, and R. K. Saxena, J. Appl. Math. **2011**, 298628 (2011).